Journal of Engineering Physics and Thermophysics, Vol. 72, No. 6, 1999

NUMERICAL STUDY OF ASTEROID IMPACT ON THE EARTH'S SURFACE WITH ALLOWANCE FOR GRAVITATION AND RADIATION ENERGY TRANSFER

G. S. Romanov and A. S. Smetannikov

UDC 533.6.01

The study presents a procedure for numerical modeling and results of gasdynamic calculations of asteroid impact on the surface in a two-dimensional axisymmetric formulation for impact velocities of ~50 km/sec and asteroid dimensions of ~ 1 km. The effect of gravity and radiation energy transfer are taken into account. Radiation transfer is calculated using the equations of radiation diffusion in the multigroup approximation with respect to the photon energy (10 spectral groups). The equations of radiation diffusion are solved by the method of alternating directions.

The dynamics of the processes occurring in a high-velocity asteroid impact on the surface of the planets is now under active study. These investigations are of interest for many problems of astrophysics and space physics, including the consequences of possible fall of large space objects on the earth. Experimental data on high-velocity impact belong to the region of velocities not higher than 20 km/sec. The region of impact velocities of the order of 100 km/sec is practically inaccessible to experimental study. In this connection, theoretical study of the dynamics of impact gains particular importance. Study [1] carried out two-dimensional numerical modeling of the dynamics of the flow arising from asteroid impact on the ground with a velocity normal to the surface. These calculations were made for a homogeneous atmosphere and ground. The current work is an elaboration of [1] and accounts for gravity (and, hence, for atmosphere and ground inhomogeneity) and the effect of radiation energy transfer on the flow dynamics and parameters.

The flow arising from high-velocity asteroid impact on the ground is described using gasdynamic equations for the axisymmetric case in $r-z$ coordinates:

$$\rho\left(\frac{\partial u}{\partial t}+v\frac{\partial u}{\partial r}+u\frac{\partial u}{\partial z}\right)=-\frac{\partial P}{\partial z}+g,\quad \rho\left(\frac{\partial v}{\partial t}+v\frac{\partial v}{\partial r}+u\frac{\partial v}{\partial z}\right)=-\frac{\partial P}{\partial r},$$

$$\frac{1}{\rho}\frac{d\rho}{dt}=-\left[\frac{1}{r}\frac{\partial (rv)}{\partial r}+\frac{\partial u}{\partial z}\right],\quad \rho\frac{d\varepsilon}{dt}=-P\left[\frac{1}{r}\frac{\partial (rv)}{\partial r}+\frac{\partial u}{\partial z}\right]+q. \tag{1}$$

This system is closed by the equations of state $P=P(\varepsilon,\rho)$ and $T=T(\varepsilon,\rho)$. For a finite-difference approximation of system (1) we employ a two-dimensional partially three-layer (with respect to velocity) fully conservative difference scheme in Eulerian cylindrical variables (r, z). The calculation of a time step is broken up into two stages, as is generally the case with the Eulerian procedure. In the first stage, momentum and energy equations whose right-hand sides retain only terms associated with the pressure and gravity and that, in fact, coincide with the equations of the Lagrangian procedure are solved. In the second stage, account is taken of terms associated with convective transfer of the pertinent quantity in the mass, energy, and momentum equations. In the same stage, final conversion is made from the parameters on the given and previous time layers to the parameters on the new time layer. To close system (1) it is necessary to specify equations of state for the media, i.e., to specify the pressure and temperature as functions of the energy and density. In the calculations we used an equation of state of the Mie–Grüneisen type in the form proposed by Tillotson [2]. Gabbroid anorthosite was taken as the meteorite and

Academic Scientific Complex "A. V. Luikov Heat and Mass Transfer Institute," National Academy of Sciences of Belarus, Minsk, Belarus. Translated from Inzhenerno-Fizicheskii Zhurnal, Vol. 72, No. 6, pp. 1169-1179, November–December, 1999. Original article submitted April 28, 1999.

1062-0125/99/7206-1131$22.00 ©1999 Kluwer Academic/Plenum Publishers

ground material. The difference scheme, the solution procedure, the equations of state, and the construction of the calculation grid are described in detail in [1].

In the calculations of asteroid impact on the ground, the asteroid (striker) was modeled by a cylinder of diameter D and length H that collides with the ground with a velocity u_0 normal to the surface. The gas–ground contact boundary lies at $z = 0$, with positive z corresponding to the gas and negative to the ground. At the initial instant of time, the meteorite comes in contact with the ground. In the calculation, at each given instant of time we determine the mass M_{ev} of cells where the specific energy is higher than the evaporation energy and the mass M_m of cells where the specific energy is higher than the melting energy.

We previously considered impact of asteroids with characteristic dimensions of the order of 1 km and velocities of ~50 km/sec with the ground [1]. The physical picture of the phenomenon is the following. At the site of impact, the pressure rises rapidly and attains a maximum. Two shock waves (SW) appear – one goes into the ground and the other propagates along the asteroid (striker) body opposite to its motion. The latter wave quickly raises the specific energy of the striker material and evaporates it. Subsequently, this wave passes to the atmosphere and ascends, gradually expanding radially. Behind the asteroid body moving into the ground, a rarefied region is formed, into which the surrounding medium flows. Subsequently, accumulation of this flow on the symmetry axis occurs, and as a consequence, the density of internal energy (and the temperature) in this region rises significantly. Thus, a hot region is formed behind the front of the shock wave moving into the gas. The shock wave moving into the ground raises the parameters in the surrounding medium and evaporates the ground (as long as its intensity is sufficient for this). This shock wave is followed by the asteroid, which slows down and gradually deforms. The penetration of the asteroid into the ground gives rise to a crater, and the asteroid material spreads over its surface. By this instant of time, the meteorite body has turned inside out – the outer surface of the striker (making contact with the gas at the initial instant of time) becomes the inner, and the inner surface (making contact with the ground at the initial instant of time) becomes the outer. An upward jet appears around the edge of the crater formed. The jet consists of material of both the asteroid and the ground involved in this movement. As a result of the deceleration of the asteroid, a significant portion of the kinetic energy converts into internal energy, and a second region with a high temperature and energy is formed inside the crater. Subsequently, the shock wave in the gas rises and expands radially. The lower boundary of the asteroid reaches a maximum depth and stops. The material near the upper boundary of the asteroid in the crater starts moving toward the gas. Rayleigh–Taylor instability is likely to develop here, since denser material accelerates toward less dense. The crater grows gradually. The shock wave in the ground reached a significant depth and acquired a hemispherical shape, and its parameters decrease with time. The subsequent development of the flow leads to enlargement of the region covered by the flow and to a gradual decrease in the maximum parameters.

To take account of the effect of gravity, the acceleration due to gravity g is added to the right-hand side of the equation of motion. In the gas use is made of the model of an isothermal exponential atmosphere $\rho = \rho_0 \exp(-z/L)$ with a characateristic height $L = 7.9$ km ($\rho_0 = 1.29 \cdot 10^{-3}$ g/cm^3 is the density of air at $z = 0$). In the ground, the pressure is constructed such that its gradient counterbalances the weight of the overlying layers. Here, we employ the difference approximation of the balance equations $dP/dz = \rho g$ with account for the equations of state and adiabatic compression of the ground $d\varepsilon = -Pd(1/\rho)$.

We now consider results calculated for impact of an asteroid with $D = H = 1$ km with the ground with a velocity $u_0 = 50$ km/sec with allowance for gravity (the first version). The initial phase of the impact (penetration of the asteroid body into the ground, its deceleration and stoppage) practically does not differ from the calculation with a homogeneous atmosphere and ground, in view of which we will not describe it in detail. Figure 1a plots density, energy, pressure, temperature, and velocity fields for the time $t = 0.3$ sec. On the density field it is clearly seen that the crater depth at this instant of time is 4 km and the crater radius is slightly larger than 2 km. The shock wave in the ground reached a depth of 4.7 km, its radial dimension is 4 km, and the maximum pressure is equal to 400 kbar. In the hot region inside the crater, the specific energy has a maximum of 118 kJ/g, and the maximum temperature is 12.3 eV. The shock wave in the gas rose to a height of 6 km and reached 3 km in radius. The energy and temperature maxima in it are significant, 123 kJ/g and 12.7 eV. The maximum radial and axial velocities are as follows: $u = -4$ km/sec and $v = 2.1$ km/sec in the ground shock wave, and $u = 34$ km/sec and v

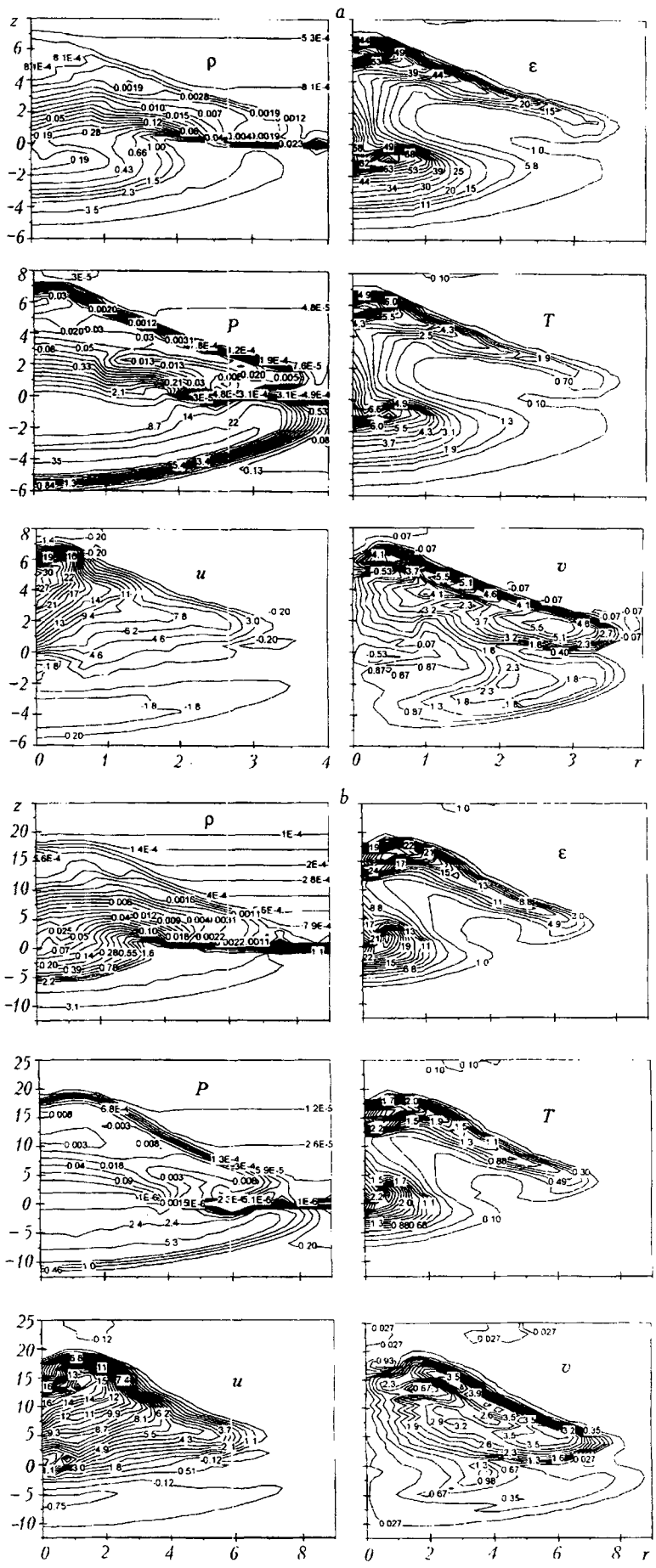
a
z
ρ
ε
P
T
u
v
r
b
z
ρ
ε
P
T
u
v
r

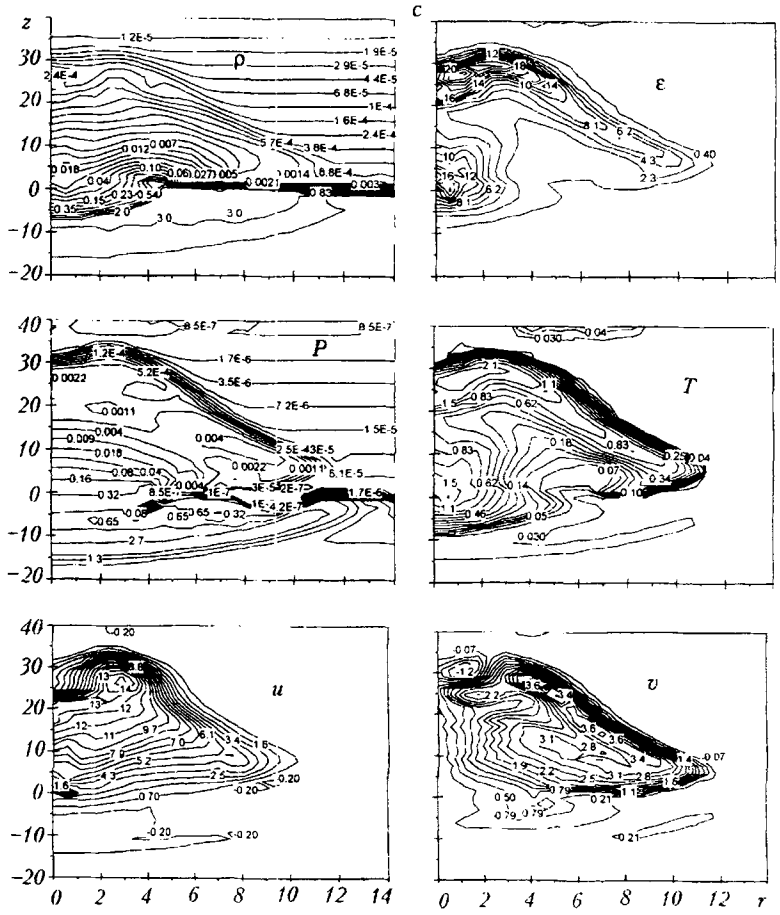

Fig. 1. Density, energy, pressure, temperature, and velocity fields for the first version of the calculation at the instant $t = 0.3$ sec (a), 1 sec (b), and 1.8 sec (c). z, km; r, km; ρ, kg/dm^3; ε, MJ/kg; P, GPa; T, eV; u and v, km/sec.

= 5 km/sec in the shock wave in the gas region. By the instant of time of 1 sec (the fields of the quantities are presented in Fig. 1b), the shock wave in the ground passed to a depth of 9 km, its radial dimension is more than 8 km, and the pressure maximum is equal to 90 kbar. The shock wave in the gas rose to a height of 20 km and reached 7 km in radius. Here, the maximum temperatures in the crater and gas regions are equal to about 4 eV. The crater depth is 6 km and the crater radius is 3.4 km. On the pressure and energy fields it is clearly seen that the position of the front of the shock wave in the gas on the symmetry axis (18 km) lags somewhat behind the position of the shock wave at a radius of 1.5 km (20 km). This is a consequence of the formation of a jet spouting upward around the crater edge at an earlier stage.

At the instant of 1.8 sec, the shock wave in the gas ascends to a height of 3.5 km and attains a radius of 11 km (Fig. 1c). The maximum pressure in it is 40 bar, the maximum temperature is 2.5 eV, and the maximum axial and radial velocities are 17 and 3.6 km/sec. Velocity components in the ground region are noticeably lower, being 1.8 and 1 km/sec. The crater depth increased to 6.7 km, and the crater radius, to 4.8 km. The shock wave in the ground reached a depth of 14 km and its radius is practically as much. Subsequently, the flow develops, the region covered by the flow expands, and the maximum parameters decrease gradually. By 4 sec, the SW in the gas has moved to a height of 80 km (70 km on the symmetry axis) and attained 20 km in radius. The hot region has risen from the crater to a height of 10 km, and the maximum temperature in it is already not high, 0.6 eV. In the upper hot region (at a height of 60 km), the temperature is noticeably higher, 2.1 eV, the maximum of the axial velocity is 13 km/sec, and that of the radial, 4 km/sec. The shock wave in the ground has passed 25 km and is of hemispherical shape. The crater depth is 7.5 km and the crater radius is 7 km.

Figure 2 shows the time variation of the integral flow characteristics for this version of the calculation. On the whole, their behavior is close to the calculation with a homogeneous atmosphere and ground. On penetrating

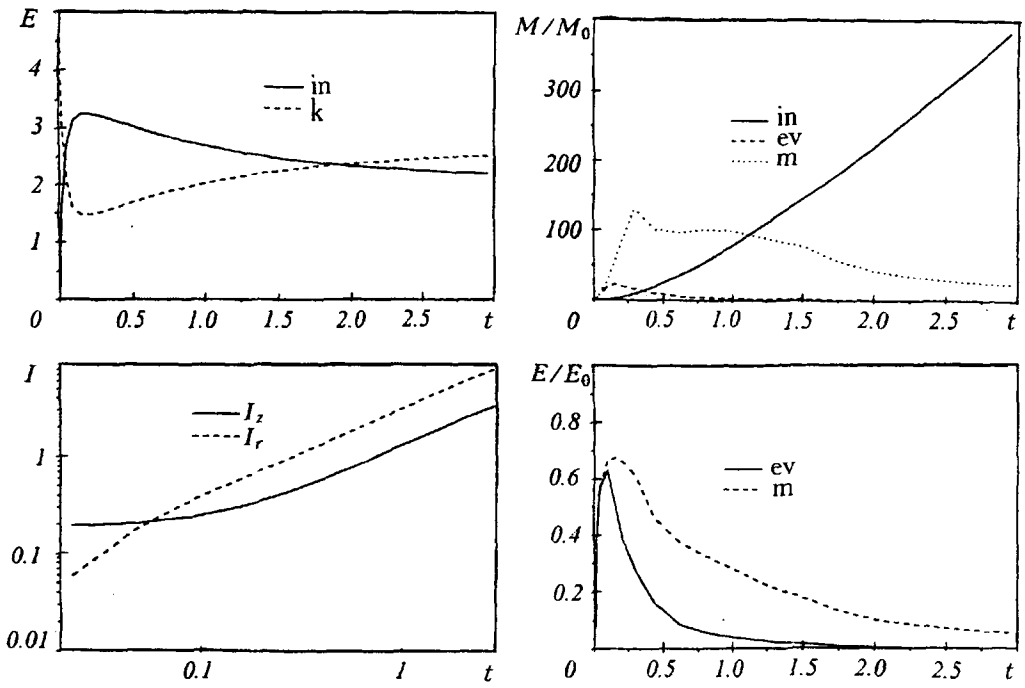

Fig. 2. Time behavior of integral characteristics for the first version of the calculation: internal (in) and kinetic (k) energies; masses evaporated (ev), melted (m), and raised above $z = 0$ (r); radial and axial momenta; energy portion in melted (m) and evaporated (ev) materials. t, sec; E, 10^{20} J; I, 10^{20} g·cm/sec.

into the ground, the striker decelerates and its kinetic energy rapidly converts into internal energy, which attains a maximum of 0.7 of the initial kinetic energy E_0 (0.16 sec). Subsequently, the internal energy falls slowly and the kinetic rises. They become equal at 1.9 sec, i.e., a little later than in the calculation without account for gravity. The evaporated mass reaches a maximum of 23.2 M_0 (0.15 sec), and the melted mass, 130 M_0 (0.3 sec). The ground mass lifted into the air above the line $z = 0$ increases in time and is about 400 M_0 by 3 sec. In addition, we calculated the material mass that can be expelled into space (i.e., that has a modulus of velocity greater than the second space velocity of 11.2 km/sec and a positive component of the axial velocity). This quantity increases slowly in time and is 0.21 M_0 by 4 sec.

As the calculations for a high-velocity impact reveal, high temperatures and large temperature gradients appear in the flow field, in which connection the energy redistribution over mass effected by radiation can play an important role in the problem. This makes it necessary to calculate radiation transfer over the flow field, and the energy equation should be supplemented with a term that accounts for the energy redistribution due to this process. Radiation transfer is calculated using the equations of radiation diffusion in the multigroup approximation [3, 4] with respect to the photon energy:

$$\operatorname{div} \vec{S} = c\kappa_l (B_l - U_l); \quad \vec{S}_l = -\frac{c}{3\kappa_l} \operatorname{grad} U_l; \quad U = \sum_l U_l; \quad \vec{S} = \sum_l \vec{S}_l. \tag{2}$$

The equilibrium radiation energy density B_l in the l-th spectral group (with boundaries with respect to the photon energy of ε_{l-1} and ε_l) is determined as follows:

$$cB_l = 4\sigma T^4 s_l, \quad s_l = \int_{x_1}^{x_2} \frac{z^3 dz}{e^z - 1}, \quad x_1 = \frac{\varepsilon_{l-1}}{kT}, \quad x_2 = \frac{\varepsilon_l}{kT}. \tag{3}$$

In cylindrical geometry in $r-z$ coordinates under the condition of axial symmetry, the system of equations (2) has the form (to simplify the writing, the index of the spectral group is omitted below)

$$\frac{1}{r}\frac{\partial (rS_r)}{\partial r} + \frac{\partial S_z}{\partial z} = c\kappa (B - U), \quad S_r = -\frac{c}{3\kappa}\frac{\partial U}{\partial r}, \quad S_z = \frac{c}{3\kappa}\frac{\partial U}{\partial z}. \tag{4}$$

Passage from these expressions to an equation of the second order yields

$$\frac{1}{r}\frac{\partial}{\partial r}\left(\frac{cr}{3\kappa}\frac{\partial U}{\partial r}\right) + \frac{\partial}{\partial z}\left(\frac{c}{3\kappa}\frac{\partial U}{\partial z}\right) + c\kappa (B - U) = 0. \tag{5}$$

The two-dimensional diffusion equation is solved numerically using various methods, namely, $\alpha-\beta$ iterations [4], alternating directions [5], conjugate gradients with the incomplete expansion of Kholetskii [6], etc. We apply the method of alternating directions, which is based on the principle of transition to a steady state. The solution of the stationary equation $\nabla(\frac{c}{3\kappa}\nabla U) = f$ is the limit as $t \to \infty$ of the solution of the equation $\frac{\partial U}{\partial t} = \nabla(\frac{c}{3\kappa}\nabla U) - f$ in the fictitious time t. Its solution is found using an iteration method, with a single iteration (passage from U^j to U^{j+1}) consisting of two time half-steps:

1) from the known U^j, the intermediate function $\tilde{U}$ is found from the equation

$$\frac{\tilde{U} - U^j}{\tau} = \frac{1}{r}\frac{\partial}{\partial r}\left(\frac{c}{3\kappa}\frac{\partial \tilde{U}}{\partial r}\right) + \frac{\partial}{\partial z}\left(\frac{c}{3\kappa}\frac{\partial U^j}{\partial z}\right) - f;$$

in the difference form, this equation is three-point in the coordinate r, and its solution $\tilde{U}$ is found using factorization along the radius.

2) from the known $\tilde{U}$, the function U^{j+1} is determined from the equation

$$\frac{U^{j+1} - \tilde{U}}{\tau} = \frac{1}{r}\frac{\partial}{\partial r}\left(\frac{c}{3\kappa}\frac{\partial \tilde{U}}{\partial r}\right) + \frac{\partial}{\partial z}\left(\frac{c}{3\kappa}\frac{\partial U^{j+1}}{\partial z}\right) - f.$$

In the difference form, this equation is three-point in the coordinate z and is solved by factorization along the axial coordinate. Conducting these iterations, we "advance" in fictitious time t until the solution reaches a steady state, which will be the solution of Eq. (5). In solving the equations on iteration half-steps, appropriate boundary conditions should, of course, be specified. The method of alternating directions is unconditionally stable (see, for example, [7]). At the same time, it is impossible to carry out the calculation with arbitrarily large time steps, since here asymptotic stability is lost. There is the possibility of selecting an optimum time step where the solution is obtained in a minimum number of steps and asymptotic stability is retained [7]. However, for this the difference operator spectrum (the set of eigenvalues) must be known, which is no less complicated a problem than solution of the initial equation. Therefore, selection of a time step should involve various heuristic considerations (stability for model problems, dimensional relations, etc.) and numerical experiments.

To solve Eq. (4) numerically, we approximate it by means of finite differences on a rectangular grid in $r-z$ coordinates, having passed to the nonstationary equation

$$\frac{1}{c}\frac{\partial U_{i,n}}{\partial t} = DU_{i,n-1} + KU_{i-1,n} + EU_{i+1,n} + VU_{i,n+1} - (C + C')\,U_{i,n} + F, \tag{6}$$

$$D = \frac{1}{(z_{i,n+1} - z_{i,n})}\,\frac{1}{2\,[\tanh 3\kappa_{i,n}(z_{i,n+1} - z_{i,n})/4 + \tanh 3\kappa_{i,n-1}(z_{i,n} - z_{i,n-1})/4]},$$

$$K = \frac{r_{i,n}}{(r_{i+1,n}^2 - r_{i,n}^2)}\,\frac{1}{[\tanh 3\kappa_{i,n}(r_{i+1,n} - r_{i,n})/4 + \tanh 3\kappa_{i,n-1}(r_{i,n} - r_{i,n-1})/4]},$$

$$V = \frac{1}{(z_{i,n+1} - z_{i,n})}\,\frac{1}{2\,[\tanh 3\kappa_{i,n+1}(z_{i,n+2} - z_{i,n+1})/4 + \tanh 3\kappa_{i,n}(z_{i,n+1} - z_{i,n})/4]},$$

$$E = \frac{r_{i+1,n}}{(r_{i+1,n}^2 - r_{i,n}^2)} \frac{1}{[\tanh 3\kappa_{i+1,n}(r_{i+2,n} - r_{i+1,n})/4 + \tanh 3\kappa_{i,n}(r_{i+1,n} - r_{i,n})/4]},$$

$$C = E + K + \kappa_{i,n}/2; \quad C' = V + D + \kappa_{i,n}/2; \quad F = (\kappa B)_{i,n},$$

the quantity $U_{i,n}$ refers to the cell center. In accordance with the method of alternating directions, a single iteration for solving Eq. (6) consists of two half-steps:

$$\frac{(\tilde{U} - U)_{i,n}}{c\tau} = DU_{i,n-1}^j + K\tilde{U}_{i-1,n} + E\tilde{U}_{i+1,n} + VU_{i,n+1}^j - C\tilde{U}_{i,n} - C'U_{i,n}^j + F, \tag{7}$$

$$\frac{(U^{j+1} - \tilde{U})_{i,n}}{c\tau} = DU_{i,n-1}^{j+1} + K\tilde{U}_{i-1,n} + E\tilde{U}_{i+1,n} + VU_{i,n+1}^{j+1} - C\tilde{U}_{i,n} - C'U_{i,n}^{j+1} + F. \tag{8}$$

We use the following as the boundary conditions. On the axis of symmetry ($r = 0$) we set $S_r = 0$. At the maximum radius of the calculation region, $S_r = cU/2$. At the minimum axial coordinate of the calculation region, $S_z = -cU/2$, and at the maximum, $S_z = cU/2$. Expression (6) was obtained using the approximation for optically thick cells where the optical thickness $3[(\kappa\Delta)_i + (\kappa\Delta)_{i-1}]/2$ in the difference representation of the flows (4) is replaced by $2[\tanh 3(\kappa\Delta_i)/4 + \tanh 3(\kappa\Delta)_{i-1}/4]$ (see [4], Ch. III, para. 5, point 3). The difference expressions for the radiation flows turn out to be the following:

$$S_{i,n}^r = \frac{U_{i-1,n} - U_{i,n}}{2[\tanh 3\kappa_{i,n}(r_{i+1,n} - r_{i,n})/4 + \tanh 3\kappa_{i-1,n}(r_{i,n} - r_{i-1,n})/4]},$$

$$S_{i,n}^z = \frac{U_{1,n-1} - U_{i,n}}{2[\tanh 3\kappa_{i,n}(z_{i,n+1} - z_{i,n})/4 + \tanh 3\kappa_{i,n-1}(z_{i,n} - z_{i,n-1})/4]}.$$

The flows refer to the centers of the pertinent cell sides.

To solve Eq. (7) by means of factorization, we introduce the factorization coefficients α^r and β^r and the coupling $U_{i,n} = \alpha_{i+1}^r U_{i+1,n} + \beta_{i+1}^r$. Using the boundary conditions on the symmetry axis $r = 0$ ($i = 2$) and at the maximum radius $r = r_{\max}$ ($i = I$), we obtain the following scheme for solving Eq. (7):

$$\alpha_2^r = 1; \quad \beta_2^r = 0; \quad \alpha_{i+1}^r = \frac{E}{C + 1/c\tau - K\alpha_i^r}; \quad \beta_{i+1}^r = \frac{K\beta_i^r + \bar{F}}{C + 1/c\tau - K\alpha_i^r};$$

$$i = 2, \ldots, I - 1;$$

$$\bar{F} = F + DU_{i,n-1}^j + VU_{i,n+1}^j + (1/c\tau - C')U_{i,n}^j;$$

$$\tilde{U}_{I,n} = \frac{\beta_I^r}{\varphi_{2,n} - \alpha_I^r}; \quad \varphi_{2,n} = \frac{1 + a}{1 - a};$$

$$a = [\tanh 3\kappa_{I,n}(r_{I+1,n} - r_{I,n})/4 + \tanh 3\kappa_{I-1,n}(r_{I,n} - r_{I-1,n})/4]/2;$$

$$\tilde{U}_{i-1,n} = \alpha_i^r \tilde{U}_{i,n} + \beta_i^r; \quad i = I, \ldots, 2.$$

Likewise, the scheme for solving Eq. (8) looks as follows:

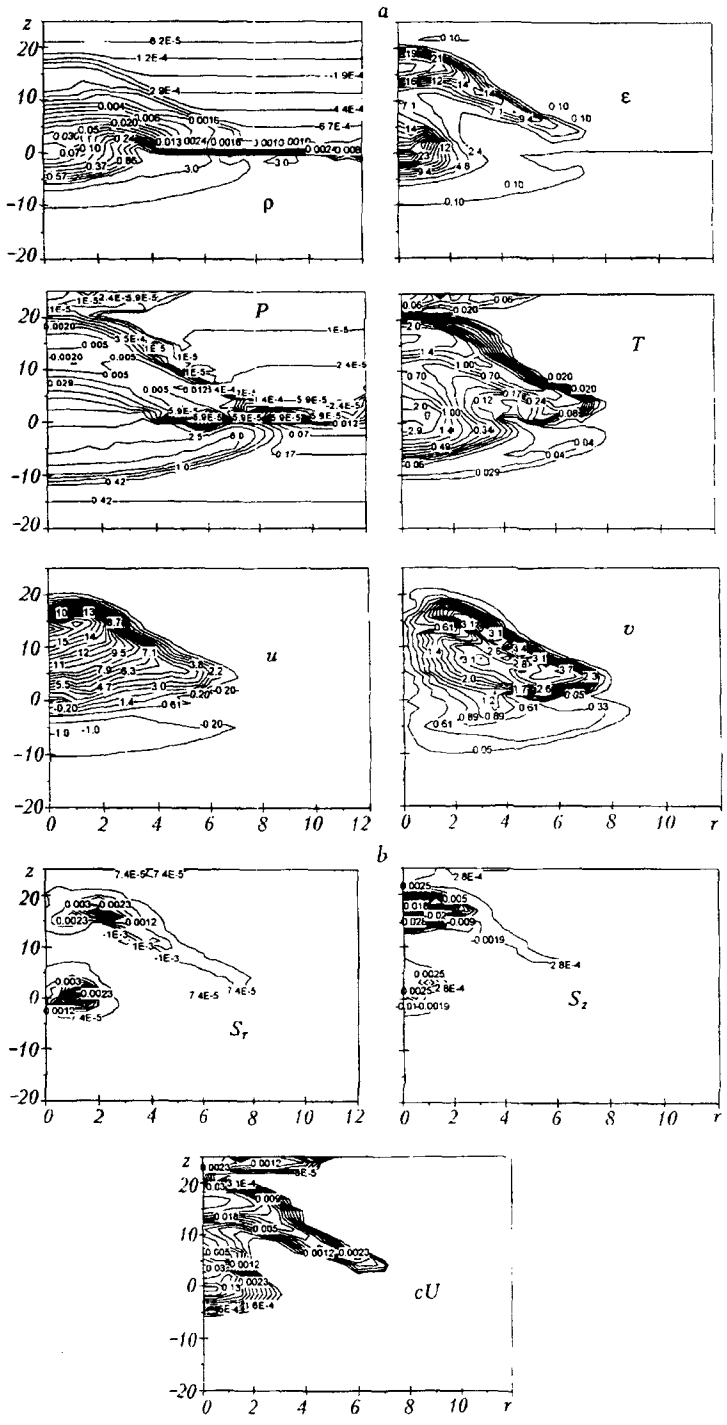

Fig. 3. Density, energy, pressure, temperature, and velocity fields (a) and fields of the radiation energy density and the radial and axial components of the radiation flow (b) for the second version of the calculation at the instant $t = 1$ sec.

$$\alpha^z_{\mathrm{NMI}} = \varphi_{3i}\,;\quad \beta^z_{\mathrm{NMI}} = 0\,;\quad \varphi_{3,i} = \frac{1-b}{1+b}\,;$$

$$b = [\tanh 3\kappa_{i,\mathrm{NMI}}\,(z_{i,\mathrm{NMI}+1} - z_{i,\mathrm{NMI}})/4 + \tanh 3\kappa_{i,\mathrm{NMI}-1}\,(z_{i,\mathrm{NMI}} - z_{i,\mathrm{NMI}-1})/4]/2\,;$$

$$\alpha^z_{n+1} = \frac{V}{C' + 1/c\tau - D\alpha^z_n}\,;\quad \beta^z_{n+1} = \frac{D\beta^z_n + \overline{F}'}{C' + 1/c\tau - D\alpha^z_n}\,;\quad n = \mathrm{NMI}, \ldots, \mathrm{NMA} - 1\,;$$

$$\tilde{F}' = F + K\tilde{U}_{i-1,n} + E\tilde{U}_{i+1,n} + (1/c\tau - C)\,\tilde{U}_{i,n};$$

$$U^{j+1}_{i,\mathrm{NMA}} = \frac{\beta^z_{\mathrm{NMA}}}{\varphi_{4,i} - \alpha^z_{\mathrm{NMA}}};\quad \varphi_{4,i} = \frac{1+d}{1-d};$$

$$d = [\tanh 3\kappa_{i,\mathrm{NMA}}\,(z_{i,\mathrm{NMA}+1} - z_{i,\mathrm{NMA}})/4 + \tanh 3\kappa_{i,\mathrm{NMA}-1}\,(z_{i,\mathrm{NMA}} - z_{i,\mathrm{NMA}-1})/4]/2;$$

$$U^{j+1}_{i,n-1} = \alpha^z_n U^{j+1}_{i,n} + \beta^z_n;\quad n = \mathrm{NMA}, \ldots, \mathrm{NMI}.$$

After these computations the calculation of an iteration cycle is completed. Having conducted iterations until a steady state is reached, we obtain the solution of the equation of radiation diffusion. The condition for terminating the iterations is specified in the form $|(U^{j+1} - U^j)/U^{j+1}| \le \delta$, where δ is a constant defining the accuracy of convergence of the iterations. The energy redistribution over mass effected by radiation is described by the source in the right-hand side of the energy equation in system (1), which is determined by the divergence of the radiation flow, $q = -\mathrm{div}\,\vec{S}$.

As an example of the calculation in the approximation of radiation gasdynamics, let us consider impact of an asteroid with dimensions $D = H = 1$ km and an initial velocity $u_0 = -50$ km/sec (the second version). Here gravity is taken into account. The equations of radiation diffusion were solved using Planck absorption coefficients averaged over the photon energy in 10 spectral groups with the following boundaries: 0.015–0.511–1.41–2.71–4.51–6.52–7.95–9.96–18.6–80.5–248 eV. The absorption coefficients were calculated with allowance for bremsstrahlung, photo-, and line processes. The procedure for computing the absorption coefficients and the details of the quantum-mechanical calculations are presented in [8, 9].

The character of the flow and the fields of physical quantities at an early stage (up to about 5 sec) differ only slightly from the calculation disregarding radiation. In this connection, this stage of the flow will not be described. Figure 3 plots the density, energy, pressure, temperature, and velocity fields for $t = 1$ sec (Fig. 3a) and the fields of the radiation energy density and the radial and axial components of the radiation flow integrated over the spectrum (Fig. 3b). On the whole, the fields of hydrodynamic quantities are close to those obtained at this instant of time disregarding radiation energy transfer (see Fig. 1b). However, some differences that consist in the following are already seen. There is no lag in the SW propagating over the gas near the symmetry axis. Whereas previously the SW front on the symmetry axis was at a height of 17.5 km and rose to 20 km at a radius of 1.5 km, now it is located at a height of 20 km for radii ranging between 0 and 3 km. A heated region already begins to form before the front of the SW in the gas in the direction of the drop in the atmospheric density. This is especially clear in the diagram of the temperature field, where the SW front for heights between 12 and 20 km and radii between 2 and 5 km has widened noticeably and a heating "tongue" is formed. The temperature maximum in the SW propagating over the gas has diminished slightly and is now located on the symmetry axis, whereas previously it lay somewhat aside (at $r = 1$ km).

A similar restructuring of the temperature field has also occurred in the second hot region, i.e., near the crater. Here also, in the calculation disregarding radiation there was a temperature maximum at a certain distance from the symmetry axis ($r = 1$ km). With radiation taken into account, the temperature maximum has shifted to the symmetry axis. It should be noted that, inside the flow region with a temperature above 0.5–1 eV, the mean free paths of quanta (in all spectral groups) turn out to be markedly smaller than the dimensions of this region. And only near its boundaries does the reverse take place. As a consequence, although the radiation flows in it are large, they merely redistribute the energy internally. Radiation is carried off by noticeably smaller flows at the boundary of this region, where the temperature is lower and the mean free paths of quanta are comparable to or larger than the thickness of this "boundary" zone. At the instant of time $t = 1$ sec, the maximum radial and axial radiation flows (in absolute value) are 0.5 and 2.8 MW/cm^3, respectively. At the same time, the magnitude of the flows effecting heating is appreciably lower, of the order of several tenths of a kW/cm^2. Subsequently, the flow develops and the region it covers enlarges noticeably. The heating region ahead of the front of the SW in the gas

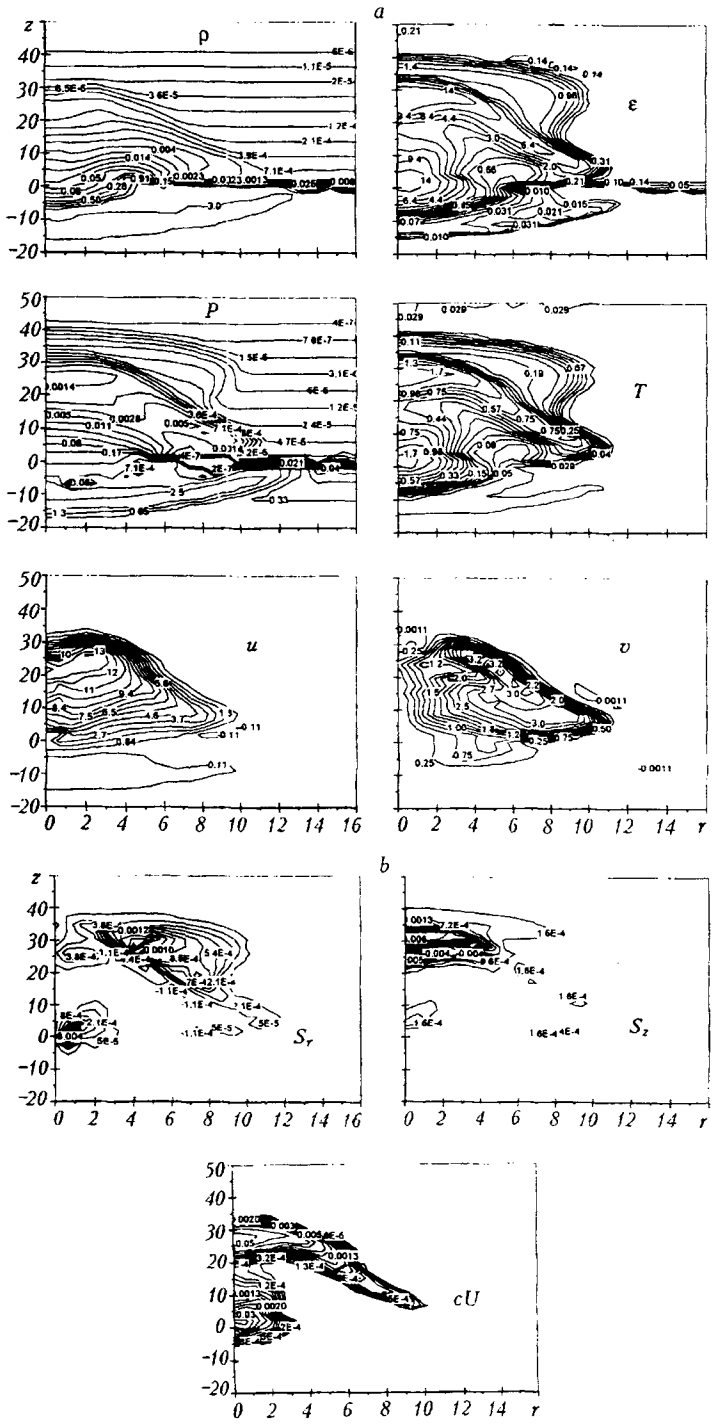

Fig. 4. Density, energy, pressure, temperature, and velocity fields (a) and fields of the radiation energy density and the radial and axial components of the radiation flow (b) for the second version of the calculation at the instant $t = 1.8$ sec.

also grows. The fields of gasdynamic quantities at the instant of time $t = 1.8$ sec are shown in Fig. 4a. Figure 4b presents the flows and the radiation energy density for this instant of time. The shock wave in the gas has risen to 3.5 km, and its radial dimension is 12 km. In the calculation with radiation, the temperature maximum in the gas has decreased to 1.9 eV (in the gasdynamic calculation it was 2.3 eV). Due to radiation, a wide heating zone with a thickness of about 5 km and a temperature of the order of 0.3 eV has formed ahead of the SW front. This is readily traced in a comparison with the temperature and pressure fields (see Fig. 3) at the same instant of time in the calculation without radiation transfer. This heating gives rise to a wave in the pressure field running ahead

of the SW front in the region of exponential decrease of the atmosphere. At the same time, should the atmosphere be homogeneous (with a normal density), the heating region ahead of the front of the shock wave in the gas would be very narrow and practically unnoticeable on the overall background of a decrease in the parameters ahead of its front, i.e., allowance for gravity causing the gas density to decrease with height is also important. This heating wave does not practically affect the density field. The maximum temperature in the "near-crater" hot region increases somewhat, by about 0.2 eV. At $t = 1.8$ sec, the maximum radiation flows have a value of 400–600 kW/cm^2; however, heating (energy removal from the hot region) is effected by flows that are about an order of magnitude smaller. The time behavior of integral characteristics has remained practically the same as in the calculation without radiation transfer. The energy removed from the flow region by radiation accounts for a small portion ($\sim 10^{-4}$) of the initial kinetic energy of the asteroid.

The following is noted in conclusion. A computational program for two-dimensional gasdynamic problems based on fully conservative difference schemes in Eulerian coordinates with consistent approximation of the flows is worked out. Asteroid impact is modeled with allowance for gravity (the atmosphere is isothermal exponential, and the pressure gradient in the ground counterbalances the weight of overlying layers). In this case, the calculations are carried out both in the gasdynamic approximation and with account for radiation energy transfer. The effect of gravity on the time behavior of integral characteristics of the impact proves to be insignificant. Radiation transfer gives rise to a wide heating region with a temperature of the order of 0.3 eV ahead of the front of the shock wave in the gas (on the side of the exponential decrease of the atmosphere). Radiation energy transfer alters somewhat the parameters inside the region covered by the flow and the shape of the front of the shock wave moving over the gas.

The work was carried out under the program of the International Science and Technology Center, project B23-96.

NOTATION

r, z, coordinates; t, time; v, u, radial and axial velocities; ρ, density; P, pressure; ε, energy of unit mass; T, temperature; U, radiation energy density; $\vec{S}$, S_r, S_z, radiation energy flow and its radial and axial components; σ, Stefan–Boltzmann constant; k, Boltzmann constant; κ, absorption coefficient; c, speed of light. Subscripts: i, number of a point on the radius; n, number of a point on the axis; j, number of a time layer; ev, evaporated; m, melted; NMI, NMA, minimum and maximum indices of the calculation region along the coordinate z; 2 and I, minimum and maximum indices of the calculation region along the coordinate r; l, number of a spectral group.

REFERENCES

1. F. N. Borovik, G. S. Romanov, and A. S. Smetannikov, *Inzh.-Fiz. Zh.*, 72, No. 4, 686-696 (1999).
2. J. D. O'Keefe and T. J. Ahrens, in: *Proc. 6th Lunar Sci. Conf.* (1975), pp. 2831-2844.
3. Ya. B. Zel'dovich and Yu. P. Raizer, *Physics of Shock Waves and High-Temperature Hydrodynamic Phenomena* [in Russian], Moscow (1967).
4. B. N. Chetverushkin, *Mathematical Simulation of Problems of the Dynamics of an Emitting Gas* [in Russian], Moscow (1985).
5. D. W. Peaceman and H. Rachford, *SIAM J.*, 3, No. 1, 28-41 (1955).
6. D. Kershaw, *J. Comp. Phys.*, **26**, No. 1, 43-65 (1978).
7. R. P. Fedorenko, *Introduction to Computational Physics* [in Russian], Moscow (1994).
8. G. S. Romanov, L. K. Stanchits, and K. L. Stepanov, *Zh. Prikl. Spektrosk.*, 30, 35-43 (1979).
9. G. S. Romanov, K. L. Stepanov, and M. I. Syrkin, *Opt. Spektrosk.*, 47, 860-868 (1979).